Journal of Geoscience and Environment Protection, 2023, 11, 201-217
https://www.scirp.org/journal/gep
ISSN Online: 2327-4344
ISSN Print: 2327-4336

Geochemical Signature and Metalogeny of BIFs and Associated Iron Ore of Zatua Hills, Haut-Uele Province (DR Congo)

Levesque Makuku Mbo[1,2,3*], Dominique Wetshondo Osomba[1,3], Valentin Kanda Nkula[1,2], Kelly Nzambe Keyila[3], Albert Ongendangenda Tshiende[1]

[1]Department of Geosciences, Faculty of Science and Technology, University of Kinshasa, Kinshasa, DR Congo
[2]Geological and Mining Research Center (CRGM), Kinshasa, DR Congo
[3]Faculty of Oil, Gas and Renewable Energies, University of Kinshasa, Kinshasa, DR Congo
Email: *levmakuku@gmail.com

How to cite this paper: Mbo, L. M., Osomba, D. W., Nkula, V. K., Keyila, K. N., & Tshiende, A. O. (2023). Geochemical Signature and Metalogeny of BIFs and Associated Iron Ore of Zatua Hills, Haut-Uele Province (DR Congo). *Journal of Geoscience and Environment Protection, 11,* 201-217.
https://doi.org/10.4236/gep.2023.1110014

Received: July 21, 2023
Accepted: October 22, 2023
Published: October 25, 2023

Abstract

Zatua Hills are located in the northeastern part of the DR Congo in Haut Uélé Province, formerly known as Province Orientale. This part of DR Congo is identified by the high elevated zone, which has remained a witness to a stable zone not affected by the ancient erosion process. BIFs are most abundant and are dated to the Neoarchaean and Late Kibalian, hosted in the Upper Congo Granites Massifs of the DR. Congo. Zatua Hills consist of dolerite, phyllade, clay-rich sediment, poor itabirite, enriched BIFs, friable hematite, hard hematite, and mineralized and unmineralized breccias. Field study and geochemistry analysis by XRF, XRD, and ICP-MS are executed in order to know the geochemistry signature and paragenesis of Zatua Hills and the probably process could lead the BIFs to iron ore. The geochemistry analysis by XRF, XRD, and ICP-MS shows that Iron ore content has an iron rate between 57% and 69% with less deleterious elements such as Si, P, and Al. These deleterious elements are secondary and have silicium composition (probably quartz or chert, goethite, and Kaolinite), aluminum (probably gibbsite, variscite, cadwaladérite, goethite, and Kaolinite), phosphorous (probably variscite), and hydrated minerals, which are grown LOI in the samples. Hypogen and supergen processes are played in BIFs for iron ore conversion and, respectively, silica dissolution and leaching. Metamorphism was also impacted and marked by the Ti element (anatase) in samples, contributing to the crystallization of martite to hematite after magnetite oxidation.

Keywords

BIFs, Zatua Hills, Geochemestry, DRC, Iron Ore

1. Introduction

The Northeastern part of the DRC has immense iron resources that can reach tens or even hundreds of billions of tons, capable of initiating its industrialization policy and providing iron-based materials and alloys necessary for the needs of Central Africa, a potential market for road construction and civil engineering works. These resources are mainly related to the itabirite formations contained within the greenstone belt of the NE part of the DRC, including those of Ngayu, Zani, Kilo, Moto, Mambasa, Panga, Tele, and Isiro, which constitute the Kibalian series contained in most of the granitic massifs of the "Upper Congo Granites Complex," which are divided into an Early Kibalian, consisting of high-grade metamorphic series, basaltic-type volcanic rocks, and tonalite intrusions (>2.8 Ga) with a scarcity of BIFs and metasediments (Lavreau, 1984). And a Late Kibalian, dominated by metasediments, large volumes of BIFs, rare volcanic rocks, and intruded by granitic rocks (>2.45 Ga) (Lavreau & Ledent, 1975; Lavreau, 1980). The main accumulations of these BIFs form high and very noticeable topography surfaces in the region, namely: the Tina, Maie, Asonga, Zatua Hills, etc. In this publication, we focus on studying the BIFs of the Zatua Hills, characterized by a relatively smaller plateau with altitudes ranging from 500 to 1089 m. Chains and intermittent hills can rise up to 300 m above the surrounding plateau.

The target area consists of a series of NW-SE trending hills, within which lies the Zatua Hills with a maximum elevation of 1300 m. To the southeast, the area is bordered by the Western Rift Valley, including Albert and Edward Lakes, separated by the Rwenzori Hills (5119 m).

Northeastern DRC occupies both the northeastern part of the Congo Basin and the elevated areas that constitute the western boundaries of the graben (rift) basin. This region, essentially composed of Archean shields, is covered by a series of Neoproterozoic and Phanerozoic formations that are affected by the aftershock of recent Cenozoic tectonic events that gave rise to the East African Rift.

In this study, we will present geochronological data from the various sites visited, with a focus on the metallogenic aspects and its significance for the quality of iron ore for metallurgical industries.

2. Study Area

2.1. Geographical Context

The Zatua Hills, which are the subject of this publication, are located between the Bafwasende Degree Square in the north and the Isiro (Paulis) Degree Square

in the south, and are situated between 27˚31'48" and 27˚40'48" East longitude and between 1˚55'48" and 2˚01'48" North latitude. They are located in the Wamba Territory, Haut-Uélé Province in the Democratic Republic of the Congo, approximately 315 km by air from the city of Kisangani (Figure 1).

2.2. Geological Context

Regional geology is predominantly composed of the Archean-age basement formations covering an area of 500,000 km^2, including Uganda, South Sudan, and the Central African Republic (de Wit & Linol, 2015; de Wit & Ashwal, 1997; Cahen & Snelling, 1966). These formations were initially associated with the Tanzanian craton before being separated by the Ruwenzori chain (2 Ga) and the filling of rift basins (Borg & Shacklet, 1997; Lavreau & Navez, 1982). These formations include the Bomu amphibolitic and gneissic complex dated 3.4 - 3.7 Ga (Cahen et al., 1984), the West Nile amphibolitic complex dated 3200 Ma - 2728 Ma (Allibone et al., 2019), the Garamba complex, the granitic massifs of the Upper Congo Granites Massifs, which cover a large part of the central area, consisting

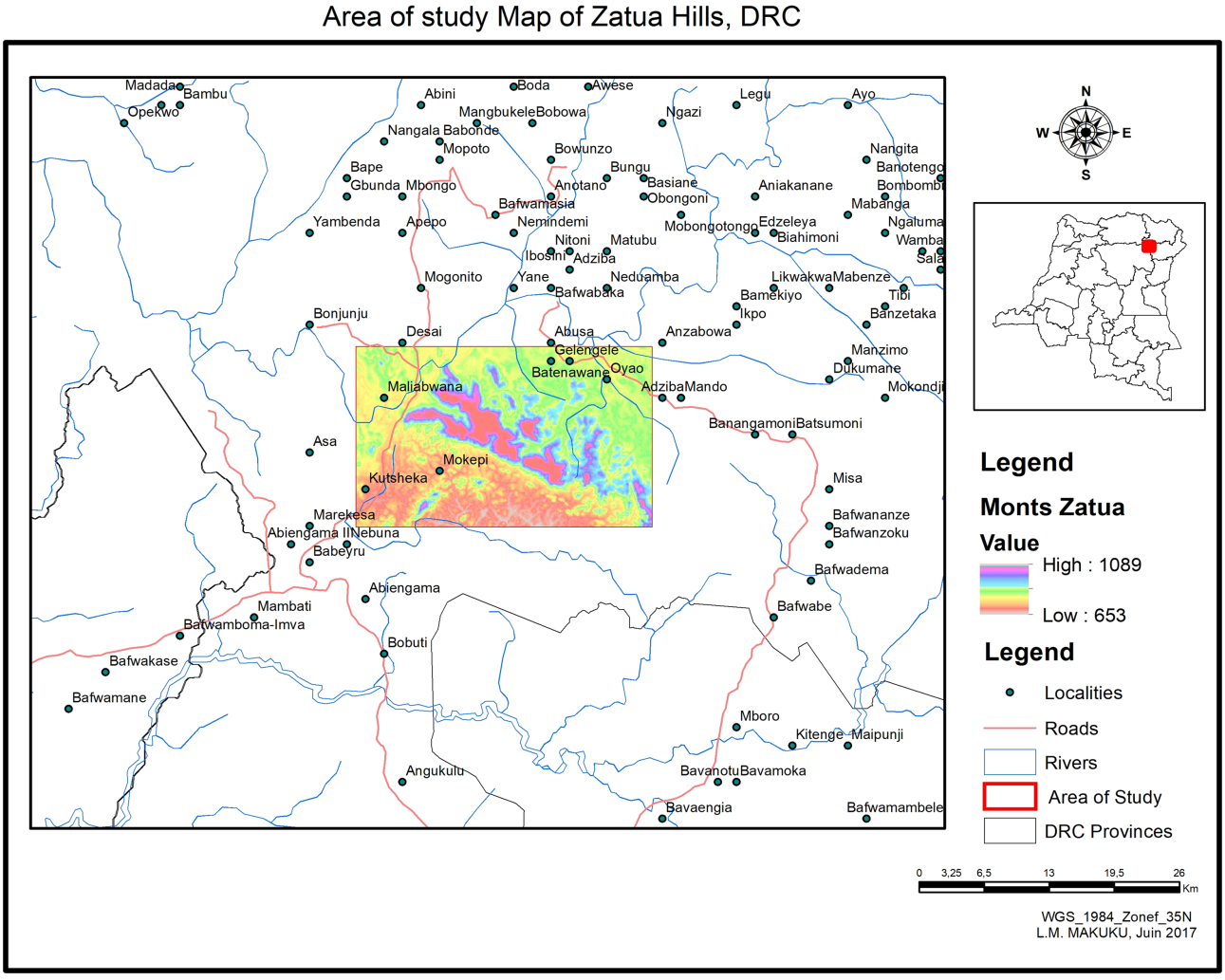

Figure 1. Location map of the study area.

of magmatic, orthogneissic and various magmatic intrusions, in which the Kibalian greenstone belt formations, including BIFs, are associated, and which form the core of the large Archean units in the region (Lavreau, 1982; Cahen & Snelling, 1966; BRGM, 1982; Cahen et al., 1984; Bird, 2016; Allibone et al., 2019).

The Zatua Hills are part of the Ngayu belt, which is one of several greenstone belts found in the Nyanza-Kibali greenstone belt, which stretches from Tanzania to the Central African Republic.

The most remarkable formations in the region are the BIFs, which occupy vast stretches compared to other geological formations. Their presence is clearly shown on the map represented in **Figure 2**. These BIFs are considered as true markers that define the different structural entities of the region. In some places, these formations can have significant thicknesses of up to 200 m, sometimes in association with certain deformations (folds, faults, laminations) and form relatively high reliefs. BIFs are sometimes found intercalated at the roof by schist rock and at the wall by basalts.

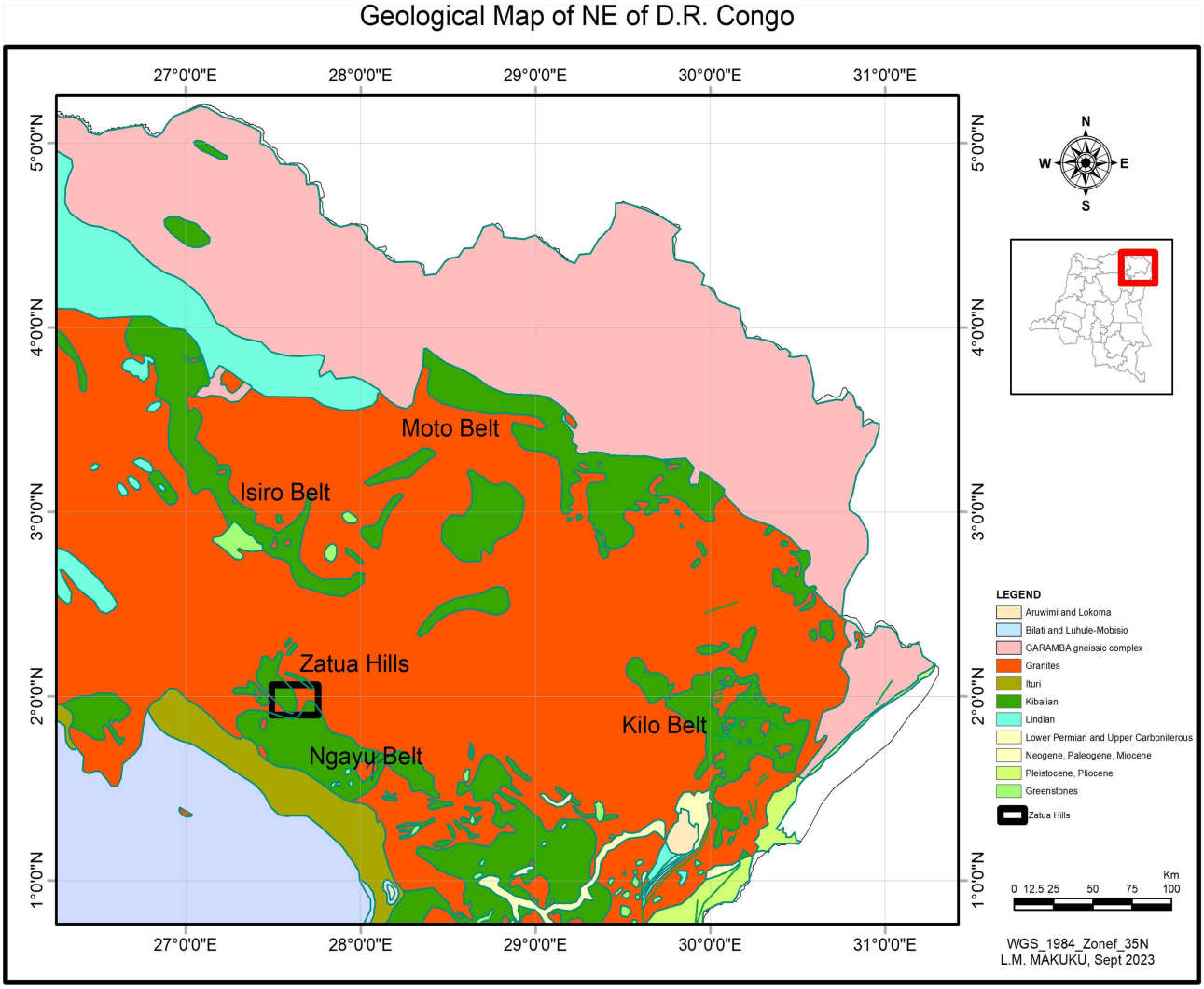

Figure 2. Geological map showing the different greenstone belts in which the BIFs of the Zatua Hills are embedded.

Apart from the BIFs, the region is also characterized by the presence of basaltic formations, intrusions of diorite, quartz monzonite and tonalite in greenstone rocks. All these rocks are covered by formations of Upper Proterozoic age (Lindian), Mesozoic formations and the West African Rift formations of Cenozoic age.

3. Methodology

This publication is a combination of a series of studies based on meticulous in situ observations, starting from multiple in situ mapping of outcrops, drilling works, laboratory geochemical analysis, and metallogenic study based on both field and laboratory results.

3.1. Field Stage

The work consisted of identifying the outcrop zones of BIFs, iron ores (enriched parts) and their host rocks using airborne magnetometric data acquired and interpreted by the company Rio Tinto, which once operated in this area, geological survey work on the relevant sites, collecting samples in the field, and mapping outcrop zones.

These data enabled the confirmation of zones with rich BIFs (% iron ≥ 50), poor BIFs (% iron < 50) and iron ores (% iron ≥ 60), not forgetting the poor host rock (% iron < 40).

Several samples were collected at these sites (Figure 3) and some were selected for geochemical analysis in the laboratory.

3.2. Lab Stage

The selected samples were used for geochemical analyses in the laboratory, specifically:

- Geochemical analyses using a Panalytical PW1840 diffractometer using Fe, Co, K filters and alpha (α) radiation to identify the predominant oxides in the drill samples;
- Geochemical analysis using X-ray fluorescence spectrophotometry (XRF) to determine major and minor elements;
- Geochemical analyses using an inductively coupled plasma mass spectrometer

Figure 3. Various surface samples selected in the Zatua Hills.

(ICP-MS) for the determination of minor elements and trace elements;

- and thermogravimetric analysis to evaluate the hydration rate (loss on ignition) of the samples from the itabirite formations and iron ore.

The geochemical analyses performed concerned twenty-six elements, but we only took into account the elements whose content was different from zero (up to 1 ppm) for all selected samples.

3.3. Interpretation and Discussion of Results Stage

The results of the geochemical analyses have enabled us to make a geochemical interpretation of the quality of BIFs of the Zatua Hills and associated iron minerals, while also considering associated elements that may influence the metallurgical quality of iron in its different stages through the formation of different alloys.

4. Results

Geological mapping and drilling work allowed the collection of numerous samples, among which 24 were selected and subjected to analysis by X-ray fluorescence (XRF), thermogravimetric analysis (LOI), and inductively coupled plasma mass spectrometry (ICP-MS) as detailed in the methodology.

The geochemical analysis results of surface samples are presented in Table 1 and Table 2, and the map below shows the different locations of the collected samples (Figure 4).

4.1. Surface Samples

4.1.1. West Zone of the Zatua Hills

The different samples collected in the Western zone of the Zatua Hills and their results are recorded in the following Tables 1-3:

Table 1. Results of geochemical analysis by fluorescence (XRF) of oxides of the iron ore samples from the Western zone of the Zatua Hills.

Elts (%)/Samples.	Fe_2O_3	SiO_2	Al_2O_3	TiO_2	P_2O_5	CaO	MgO	LOI	Rock type
MZ018	99.05	0.35	0.12	0.005	0.071	0.01	0.01	0.14	BIFs
MZ019	99.02	0.45	0.1	0.005	0.080	0.01	0.06	0.28	BIFs
MZ020	98.68	0.46	0.28	0.005	0.027	X	0.03	0.5	BIFs
MZ021	97.45	0.72	0.46	0.005	0.103	0.01	0.05	0.84	BIFs
MZ023	97.25	0.66	0.44	0.01	0.119	0.01	0.01	1.33	BIFs
MZ024	95.56	1.5	1.39	0.12	0.041	0.02	0.03	1.09	BIFs
MZ017	93.63	1.35	2.68	0.11	0.080	X	0.02	2.1	Iron Breccia
MZ016	93.43	0.91	1.96	0.05	0.147	X	0.01	3.25	BIFs
MZ015	91.49	1.03	3.61	0.17	0.144	X	0.03	3.17	Iron Breccia
MZ022	90.84	2.98	3.1	0.2	0.112	0.01	0.01	2.44	BIFs

X: Content lower than 0.001 ppm.

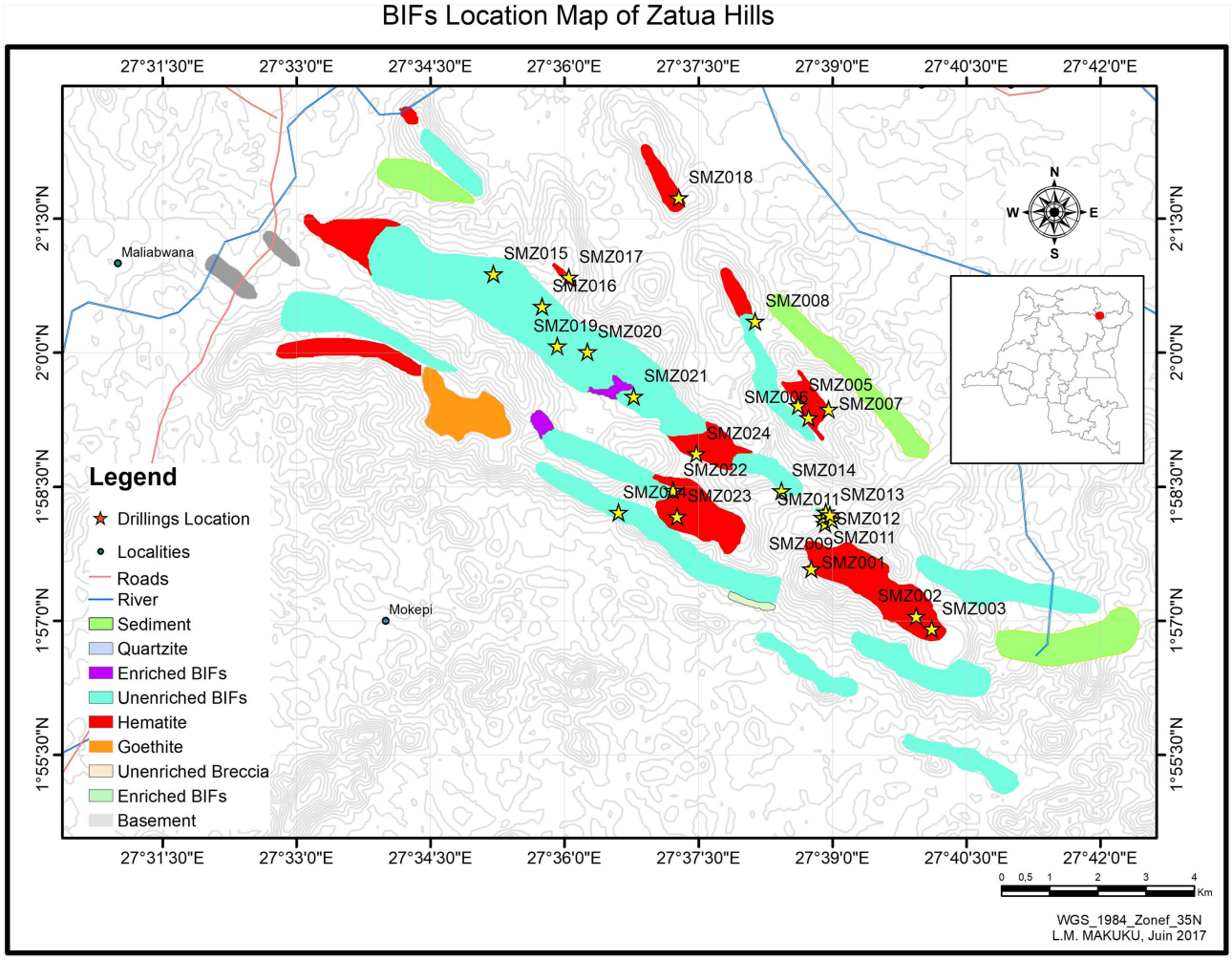

Figure 4. Sampling map.

Table 2. Results of geochemical analyses using an Inductively Coupled Plasma Mass Spectrometer of some elements in the iron ore samples from the Western zone of the Zatua Hills.

Elts (%)/Samples.	Fe	Cl	S	Ba	Mn	Ni	Sn	Sr	V	Zr	As
MZ018	69.28	0.015	0.004	0.007	0.02	0.001	0	0.01	X	X	0.003
MZ019	69.26	0.014	0.006	0.008	0.04	0.001	0	0.01	0.003	0.001	0.002
MZ020	69.02	0.014	0.004	0.005	0.05	5E−04	0	0.01	0.002	X	0.003
MZ021	68.16	0.022	0.004	0.005	0.005	0.001	0	0	0.002	X	0.003
MZ023	68.02	0.013	0.063	0.005	0.005	0.001	0	0	0.002	X	0.002
MZ024	66.84	0.016	0.007	0.004	0.03	0.001	0	0	0.015	X	0.009
MZ017	65.49	0.008	0.024	0.008	0.02	0.001	0	0.01	0.002	0.005	0.004
MZ016	65.35	0.005	0.022	0.002	0.005	X	0	0	X	0.002	X
MZ015	63.99	0.004	0.028	0.003	0.005	x	0	0	0.003	0.005	X
MZ022	63.54	0.011	0.02	0.009	0.005	x	0	0.01	0.005	0.003	0.002

X: Content lower than 0.001 ppm.

4.1.2. East Zone of the Zatua Hills

The various samples collected in the Western Zone of the Zatua Hills and their results are recorded in Table 3 and Table 4 below:

Table 3. Geochemical analysis results using X-ray fluorescence (XRF) of the iron ore oxide samples from the East zone of Monts Zatua.

Elts (%)/Samples	Fe_2O_3	SiO_2	Al_2O_3	P_2O_5	TiO_2	CaO	MgO	LOI	Rocks Type
MZ014	98.84	0.4	0.12	0.041	0.005	0.01	0.005	0.23	Iron ore
MZ005	98.75	0.54	0.18	0.048	0.005	0.01	0.02	0.27	Iron ore
MZ009	98.56	0.57	0.27	0.032	0.005	0.01	0.005	0.4	Iron ore
MZ003	98.05	0.83	0.47	0.073	0.01	0.005	0.12	0.59	Iron ore
MZ001	97.46	0.47	0.76	0.197	0.01	0.03	0.01	0.9	Iron ore
MZ012	97.23	0.74	0.84	0.461	0.01	0.02	0.01	0.71	Iron ore
MZ002	96.99	0.65	0.86	0.110	0.05	0.01	0.03	1.07	Breccia
MZ007	93.45	1.78	2.32	0.133	0.11	X	0.005	1.9	Iron ore
MZ006	91.23	0.52	5	0.101	0.1	0.02	0.005	2.73	Iron ore
MZ010	82.52	0.8	8.4	2.039	0.66	0.01	0.01	5.2	Breccia
MZ008	67.01	32.25	0.31	0.073	0.010	0.01	0.005	0.14	BIFs
MZ011	62.09	37.36	0.04	0.099	0.005	X	0.02	0.31	BIFs
MZ013	56.27	43.45	0.2	0.115	0.01	X	0.005	0.2	BIFs
MZ004	48.60	50.2	0.02	0.032	0.005	X	0.04	1.32	BIFs

X: Content lower than 0.001 ppm.

Table 4. Results of geochemical analyses using an Inductively Coupled Plasma Mass Spectrometer of several elements in iron ore samples from the Eastern area of the Zatua Hills.

Samples	*% Fe*	*% Cl*	*% S*	% Ba	% Mn	% Ni	% Sn	% Sr	% V	% Zn	% Zr
MZ014	69.13	0.026	0.001	0.008	0.02	x	0.004	0	0.002	0.002	x
MZ005	69.07	0.008	0.002	0.007	0.005	0.003	0.004	0	0.0005	x	x
MZ009	68.94	0.031	0.002	0.005	0.02	0.001	0.003	0	0.007	x	x
MZ003	68.58	0.014	0.001	0.006	0.005	0.001	0.004	0.01	0.002	x	0.001
MZ001	68.17	0.021	0.008	0.007	0.02	0.002	0.003	0.01	0.009	0.002	x
MZ012	68.01	0.014	0.011	0.02	0.005	0.002	0.002	0.03	0.012	x	0.005
MZ002	67.84	0.009	0.006	0.005	0.005	x	0.002	0	0.006	0.011	0.001
MZ007	65.36	0.009	0.019	0.012	0.005	0.01	0.002	0	0.006	x	0.001
MZ006	63.81	0.01	0.008	0.003	0.005	0.01	0.003	0.01	0.002	x	0.002
MZ010	57.72	0.008	0.031	0.011	0.02	x	0.001	0.01	0.026	x	0.028
MZ008	46.87	0.015	0.004	x	0.02	x	0.003	0.01	0.002	x	x
MZ011	43.43	0.007	0.001	x	0.005	x	0.003	0.01	x	x	x
MZ013	39.36	0.004	0.001	x	0.005	x	0.004	0.01	x	x	x
MZ004	33.99	0.004	0.001	x	0.005	x	0.002	0.01	x	x	x

X: Content lower than 0.001 ppm.

4.2. Geochemical Analysis of Sub-Surface Data (Drillings)

Samples from 4 selected surveys were analyzed via X-ray fluorescence (XRF) and thermogravimetric analysis (LOI) to determine their mineral evolution and various paragenesis associated with iron ores from prototype BIFs.

The results of the geochemical analysis are presented in the following Figures 5-13.

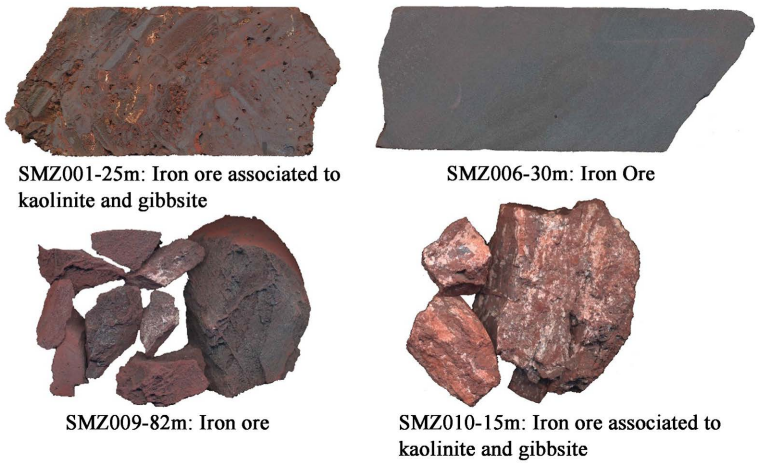

Figure 5. Various drilling samples selected in the Zatua Hills.

Borehole Samples Analysis

1) SMZ001

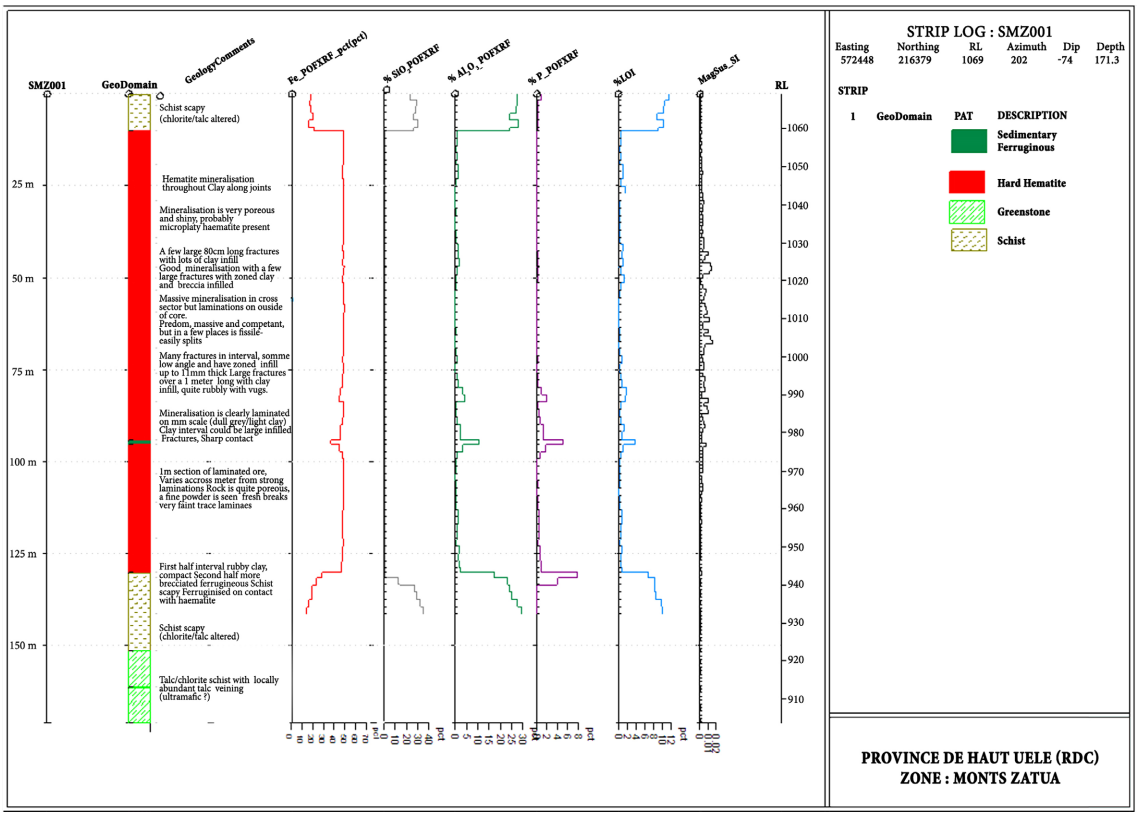

Figure 6. Lithostratigraphic and geochemical log of Borehole SMZ001.

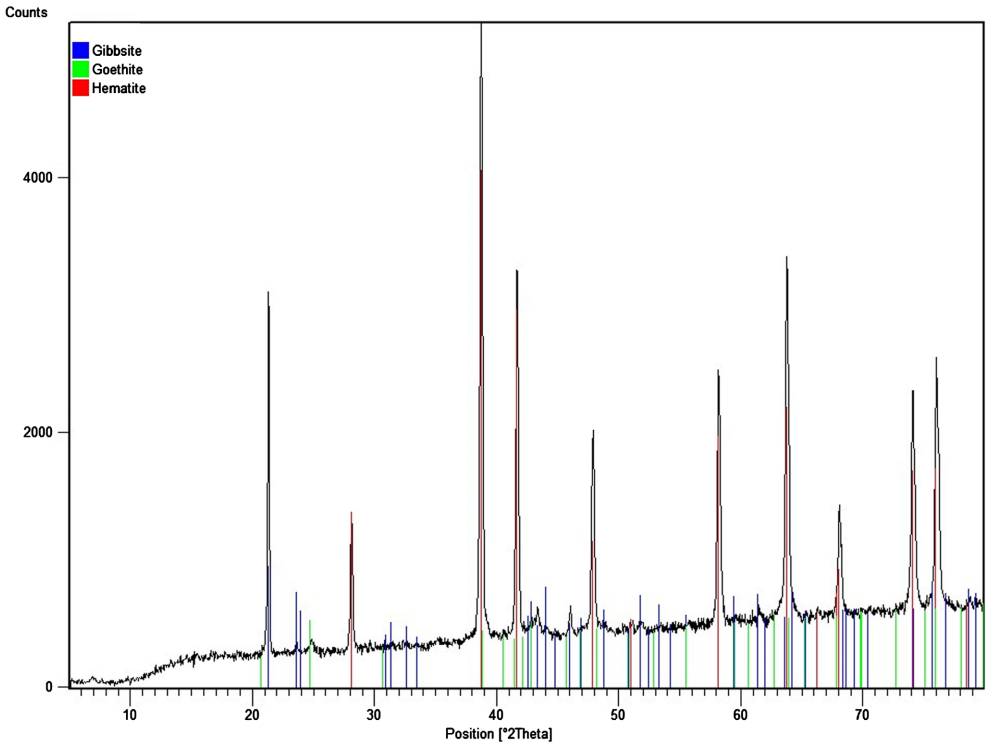

Figure 7. Diffractometric analysis showing the dominant crystals identified in sample SMZ001-25m.

2) SMZ006

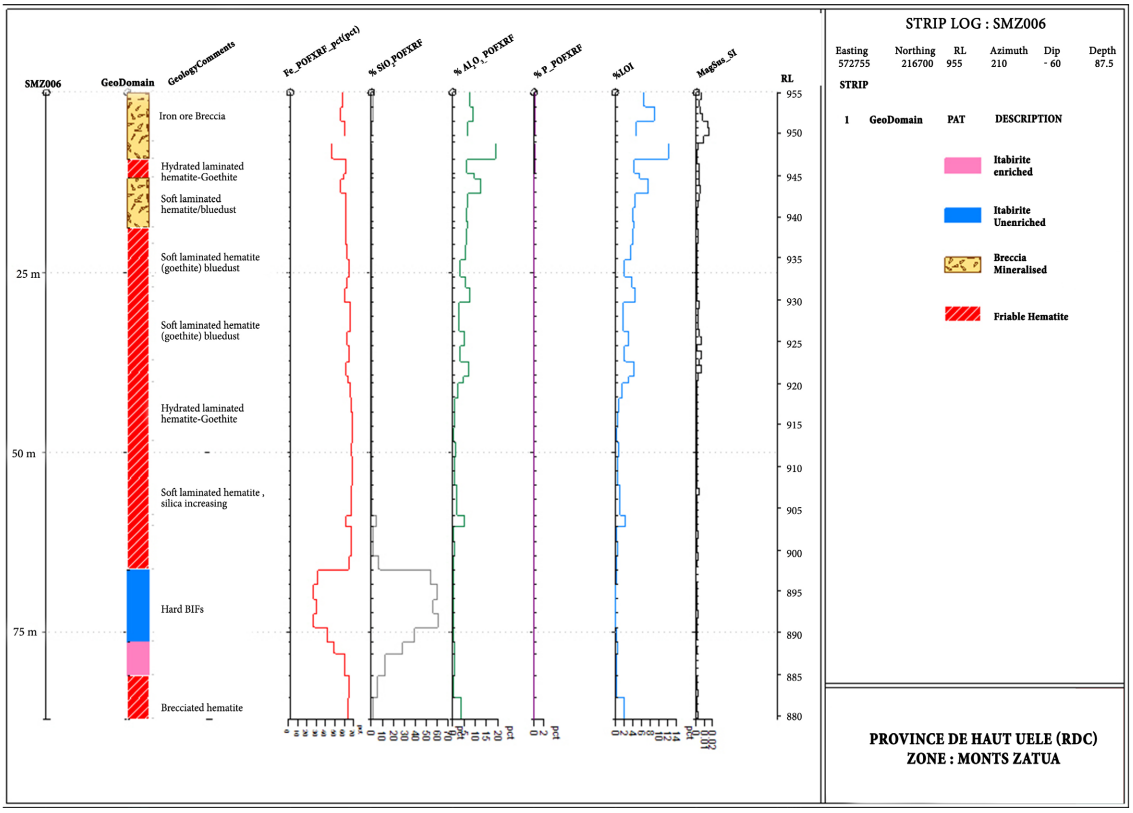

Figure 8. Lithostratigraphic and Geochemical Log of Borehole SMZ006.

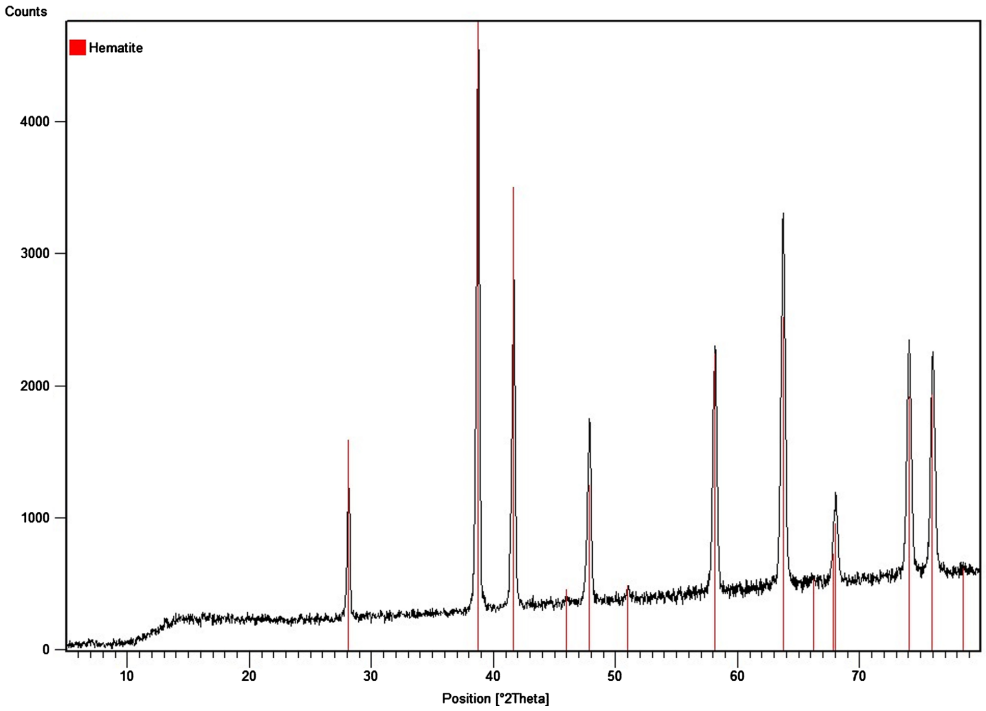

Figure 9. X-ray diffraction analysis of the sample showing the predominance of hematite in sample SMZ006-30m.

3) SMZ009

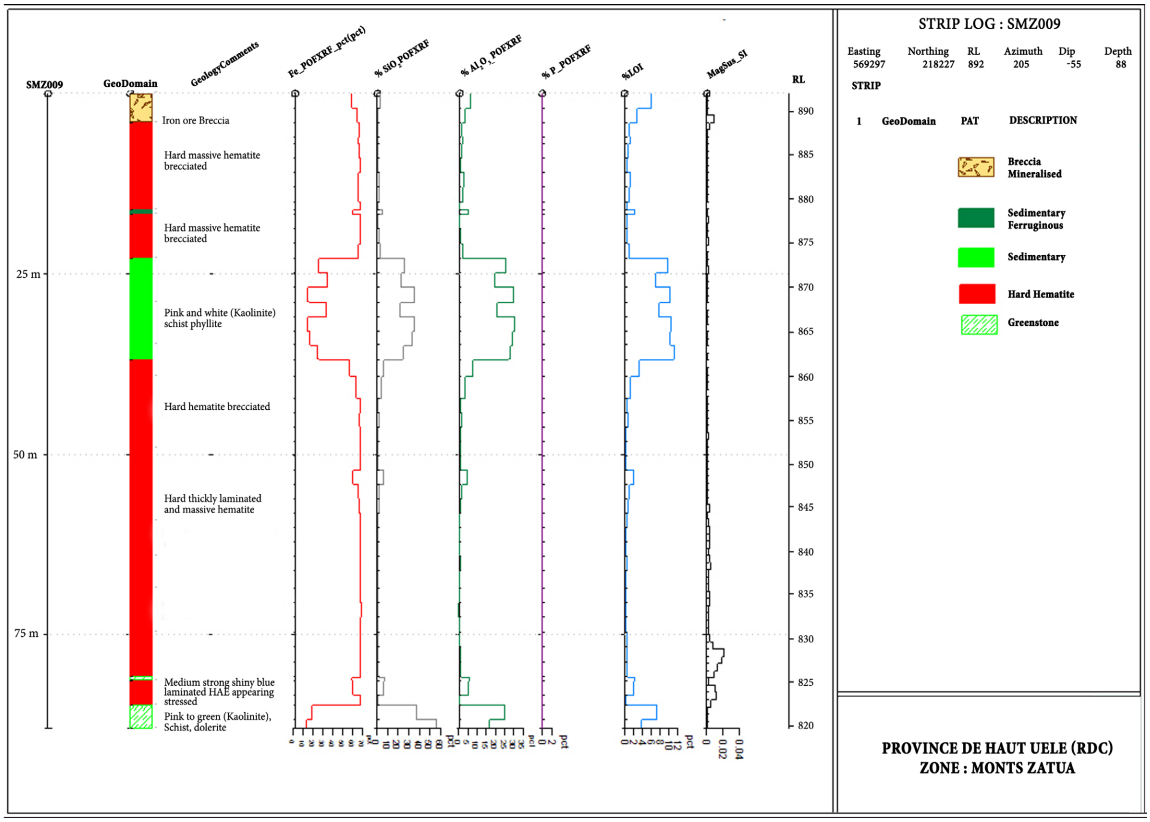

Figure 10. Lithostratigraphic and Geochemical Log of Borehole SMZ009.

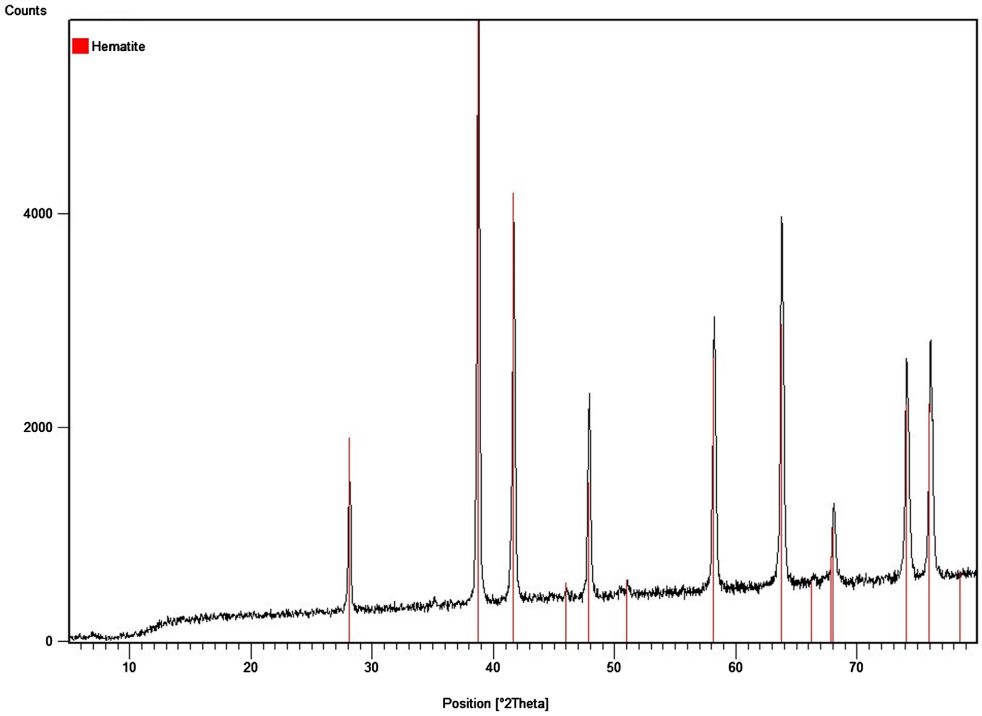

Figure 11. X-ray diffraction analysis of the sample showing the predominance of hematite in sample SMZ009-82m.

4) SMZ010

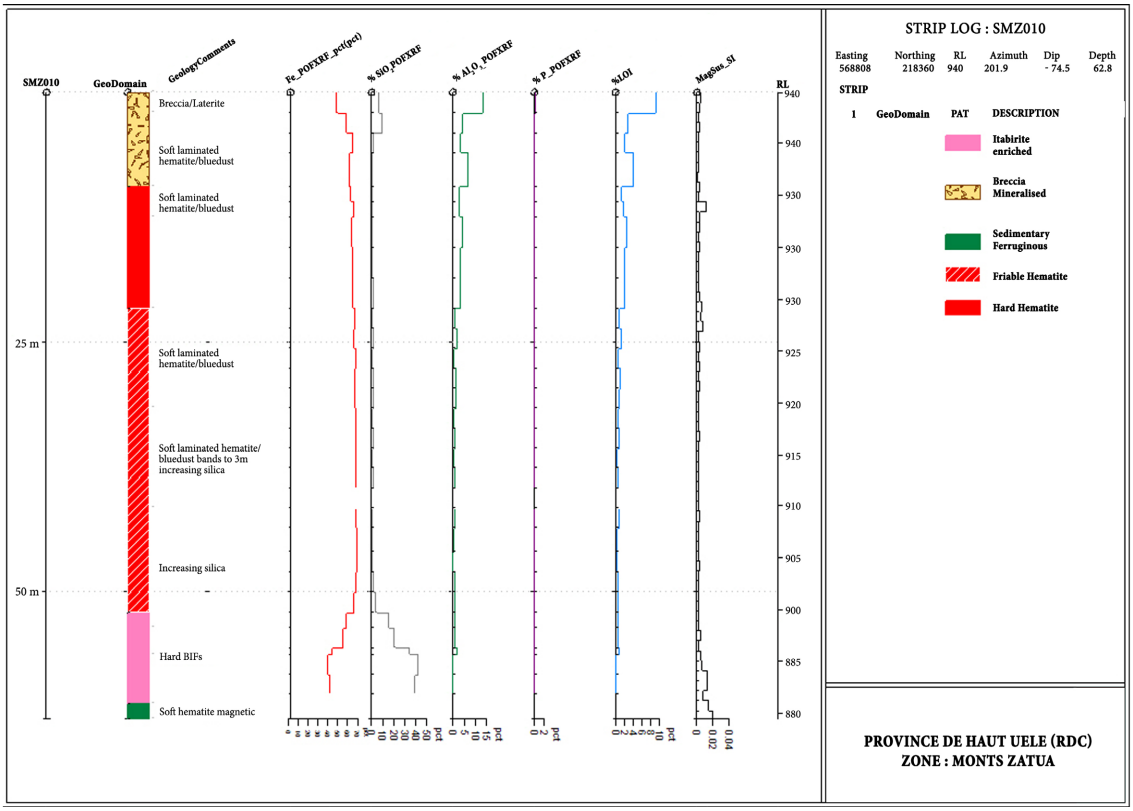

Figure 12. Lithostratigraphic and Geochemical Log of Borehole SMZ010.

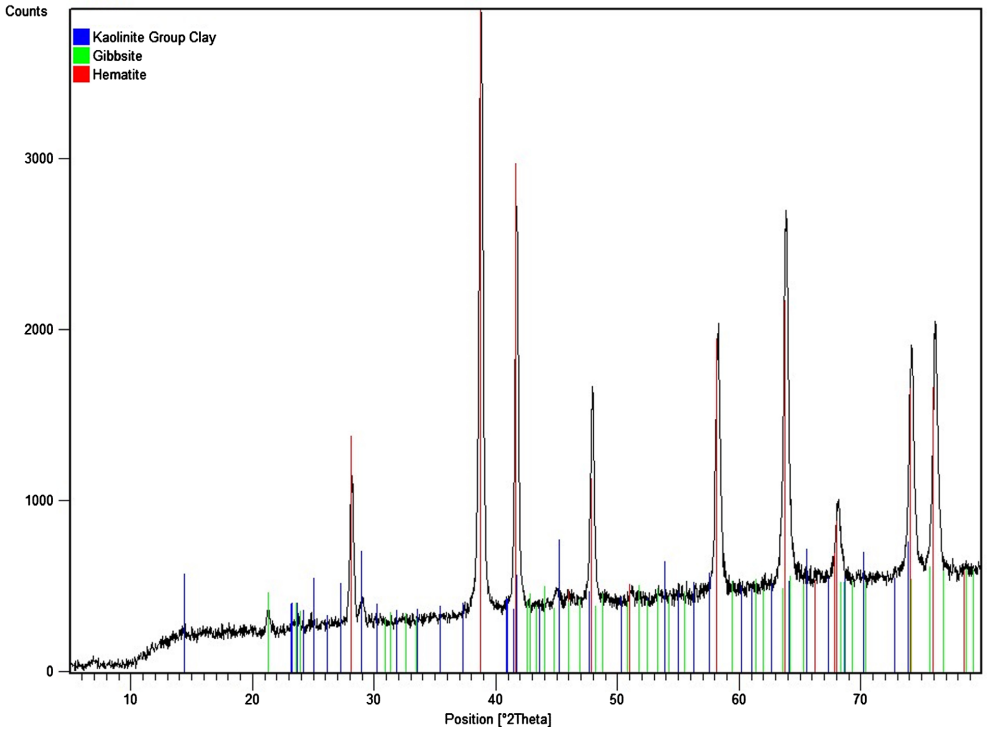

Figure 13. X-ray diffraction analysis of the sample showing the predominance of hematite in sample SMZ010-15m.

The presence of Si and Al reflects a finely-grained kaolinite within aggregates of hematite. Kaolinite and gibbsite are also abundant within microfractures traversing the rock (**Figure 10**). This sample exhibits a phyllite in the midst of ferruginization process.

5. Discussion

5.1. Geochemistry

The results of the geochemical analyses of all selected samples clearly show that for the BIFs samples whose quartz has been extensively leached and enriched with iron, the iron content varies from 57% to 69%, whereas for the unaltered BIFs, this content does not exceed 50%. This observation also holds true for other deleterious elements or impurities of iron (Al, P, and Si), which decrease in the iron ore samples compared to the BIFs.

These results clearly indicate that the majority of breccia and hematite samples are rich and do not contain Si, Al, and P levels beyond the standard, except for samples MZ001, MZ006, MZ010, MZ012, MZ015, and MZ022 which have higher than standard levels of P and Al. This excess is due to the fact that these samples were collected from fractured zones where the flow of meteoric waters has caused the circulation of secondary elements rich in Si (residual silica and kaolinite), P (solid solution of strengite-variscite), Al (gibbsite, cadwaladerite, and kaolinite), and Cl (cadwaladerite). Evidence of this circulation is the hydration rate of the rock influenced by the value of loss on ignition (LOI) in samples

where the percentage of these elements is more pronounced (Makuku, 2018).

The majority of the analyzed samples have a silica content of <1.0%, suggesting that most of the primary silica has been leached from the samples at some stage, likely during the oxidation process leading to magnetite martitization. This leaching is possible along weak zones related to rock joints, fractures, and folding, leading to the removal of primary quartz and concentration of iron minerals such as magnetite, martite, and hematite (Lascelles, 2017).

The secondary minerals in these samples are characterized by their composition in silicon (quartz or chert, goethite, and kaolinite), aluminum (gibbsite, variscite, cadwaladerite, goethite, and kaolinite), and phosphorus (variscite) in the analyses (Table 5). It is also noted that some minerals are hydrated and contribute

Table 5. Geochemical analyses of surface samples from the Zatua Hills in descending order of iron content.

Samples	%SiO_2	%TiO_2	%Al_2O_3	%Fe_2O_3	%P_2O_5	%LOI	Total	% Fe	Cl (ppm)
MZ018	0.35	0.005	0.12	99.05	0.071	0.17	**99.80**	**69.28**	150
MZ019	0.45	0.005	0.10	99.02	0.080	0.28	**100.02**	**69.26**	140
MZ014	0.40	0.005	0.12	98.84	0.041	0.23	**99.67**	**69.13**	260
MZ005	0.54	0.005	0.18	98.75	0.048	0.29	**99.86**	**69.07**	80
MZ020	0.46	0.005	0.28	98.68	0.027	0.50	**100.00**	**69.02**	140
MZ009	0.57	0.005	0.27	98.56	0.032	0.40	**99.88**	**68.94**	310
MZ003	0.83	0.010	0.47	98.05	0.073	0.59	**100.16**	**68.58**	140
MZ001	0.47	0.010	0.76	97.46	0.197	0.90	**99.86**	**68.17**	210
MZ021	0.72	0.005	0.46	97.45	0.103	0.84	**99.65**	**68.16**	220
MZ023	0.66	0.010	0.44	97.25	0.119	1.33	**99.90**	**68.02**	130
MZ012	0.74	0.010	0.84	97.23	0.461	0.71	**100.05**	**68.01**	140
MZ002	0.65	0.050	0.86	96.99	0.110	1.07	**99.79**	**67.84**	90
MZ024	1.50	0.120	1.39	95.56	0.041	1.09	99.77	**66.84**	160
MZ017	1.35	0.110	2.68	93.63	0.080	2.10	100.01	**65.49**	80
MZ007	1.78	0.110	2.32	93.45	0.133	1.90	99.73	**65.36**	90
MZ016	0.91	0.050	1.96	93.43	0.147	3.25	99.80	**65.35**	50
MZ015	1.03	0.170	3.61	91.49	0.144	3.17	99.69	**63.99**	40
MZ006	0.52	0.100	5.00	91.23	0.101	2.73	99.73	**63.81**	100
MZ022	2.98	0.200	3.10	90.84	0.112	2.44	99.73	**63.54**	110
MZ010	0.80	0.660	8.40	82.52	2.039	5.20	99.69	**57.72**	80
MZ008	32.25	0.010	0.31	67.01	0.073	0.40	100.08	**46.87**	120
MZ011	37.36	0.005	0.04	62.09	0.099	0.31	99.94	**43.43**	70
MZ013	43.45	0.010	0.20	56.27	0.115	0.20	100.27	**39.36**	40
MZ004	50.20	0.005	0.02	48.60	0.032	1.32	100.23	**33.99**	40

N.B. Samples containing SiO_2 > 3.0%, Al_2O_3 > 3.0%, and P_2O_5 > 0.18% are considered non-standard samples for metallurgical treatment.

to a high loss on ignition value.

In addition to these observations, the introduction of these secondary minerals leads to a decrease in iron content in the samples. As observed in **Table 5**, the total iron content decreases from 69.28% to 57.72% simultaneously with an increase in secondary minerals content. The nature and relative proportions of secondary minerals vary from sample to sample and may have significant implications for the industrial value of the exploited ores, particularly in the case of phosphorus.

5.2. Evidence of Elements Derived from the Hydrothermal System

When the silica in BIFs is leached by deep hydrothermal solutions, the system deposits the following elements: K and Al (stilpomelane), Rb, Sr, Ba, S (pyrite and chalcopyrite), Mg (chlorite), Ca (calcite and dolomite), and Cu (chalcopyrite). These solutions cause distal alteration around quartz veins and proximal alteration around sills and dykes (forming hard hematite). The geochemical analyses of surface and drilling samples presented in **Tables 1-5** show the presence of these elements, but at values too low to indicate the function of the hydrothermal system as a precursor to the iron ore-enrichment process (Lascelles, 2007). This is because the solubility of silica is only possible under high pressure and temperature conditions favorable to hydrothermal process (Morre & Maynard, 1929; Okamoto et al., 1957; Loughnan, 1969; Yariv & Cross, 1979; Hiemenz, 1997; Parr et al., 2003; Lascelles, 2017).

The supergene process is suggested like a recent one and follows the hypogene process that had already played a role in the solubility of primary silica, erasing the traces of the hypogene process through leaching. Metamorphism, in turn, contributed to the deconvolution and crystallization of hydrated minerals, leading to the leaching of silica and enrichment of BIFs in rich and exploitable iron ores, just like the previous processes.

This observations open the new opportunities of research by making a selection of petrographic, geochemistry, REE and others studies in order to make is place the Genetic Model of BIFS to Iron Ore in Zatua Hills.

6. Conclusion

The various analyses conducted on surface and drilling samples in the Zatua Hills area have revealed that BIFs are composed mainly by enriched Breccia, unenriched Breccia, enriched BIFs and Unenriched BIFs. In various analyses of samples of BIFs with heavily leached quartz enriched in iron, the iron content varies between 57% to 69%, whereas for unaltered BIFs, this content does not exceed 50%. Deleterious elements (Al, P, and Si) are very low in enriched BIFs and iron ores associated, and should not exceed 3% for SiO_2 and Al_2O_3 contents, and 0.18% for P_2O_5 content.

These deleterious elements coming from fractured zones where the flow of meteoric waters has caused the circulation of secondary elements rich in Si (proba-

bly residual silica and kaolinite), P (probably solid solution of strengite-variscite), Al (probably gibbsite, cadwaladerite, and kaolinite), and Cl (probably cadwaladerite). Evidence of this circulation is the hydration rate of the rock influenced by the value of loss on ignition (LOI) in samples.

This leaching is possible along zones of weakness related to rock joints, fractures, and folds, leading to the removal of primary quartz and to the concentration of iron ores (magnetite, martite, and hematite).

Magnetite, hematite, martite are the common iron minerals that exist in the samples and hematite and martite are derived by oxidation of magnetite and leaching of quartz in the BIFs.

Lascelles' modified hypogene-supergene process associated with metamorphism is suggested, in which meteoric waters and waters from the deconvolution of hydrated rocks by retrograde metamorphism played a major role in leaching silica and enriching BIFs to the exploitable rich iron ores.

The presence of Ti in the drill core samples clearly shows that it is associated with both phyllites and BIFs. Phyllites (chlorites, sericitic schists) are considered to be low-temperature metamorphic rock derived from the argillites found in this sedimentary basin. The affinity of titanium to this type of rock indicates that the associated titanium oxide form would be anatase, which corresponds to this low-temperature and low-pressure metamorphism.

Conflicts of Interest

The authors declare no conflicts of interest regarding the publication of this paper.

References

Allibone, A., Vargas, C., Mwandale, E., Kwibisa J., Jongens, R., Quick, S., Komarnisky, N., Fanning, M., Bird, F., MacKenzie, D., Turnbull, R., & Holliday, J. (2019). Orogenic Gold Deposits of the Kibali District, Neoarchean Moto Belt, Northeastern Democratic Republic of Congo. In R. H. Sillitoe, R. J. Goldfarb, F. Robert, & S. F. Simmons, *Geology of the World's Major Gold Deposits and Provinces*. Society of Economic Geologists. https://doi.org/10.5382/SP.23.09

Bird, P. J. (2016). *Evolution of the Kibali Granite-Greenstone Belt, North East Democratic Republic of the Congo, and Controls on Gold Mineralisation at the Kibali Gold Deposit* (307 p). Unpublished Ph.D. Thesis, Kingston University.

Borg, G., & Shacklet, R. M. (1997). The Tanzania and NE-Zaire Cratons. In M. J. de Wit, & L. D. Ashwal (Eds.), *Creenstone Belts* (pp. 608-619). Oxford University Press.

BRGM (Bureau de Recherches Géologiques et Minières) (1982). *A Geology and Mineral Map of Northeastern DRC Complied from by the BRGM (1980-1982) from a Field Survey in 1976 from Geological Maps Haut Zaire (Uele Area), Haut Zaïre (Ituri Area) at 1:500,000 Scale*.

Cahen, L., & Snelling, N. J. (1966). *The Geochronology of Equatorial Africa*. North-Holland Publishing Company.

Cahen, L., Snelling, N. J., Delhal, J., & Vail, J. R. (1984). *The Geochronology and Evolution of Africa* (512 p). Oxford Science Publishing, Clarendon Press.

de Wit, M. J., & Linol, B. (2015). Precambrian Basement of the Congo Basin and Its

Flanking Terrains. In M. J. de Wit, F. Guillocheau, & M. C. J. de Wit (Eds.), *Geology and Resource Potential of the Congo Basin* (pp. 19-37). Springer. https://doi.org/10.1007/978-3-642-29482-2_2

de Wit, M., & Ashwal, L. D. (1997). *Greenstone Belts* (pp. 608-619). Oxford University Press.

Hiemenz, P. C. (1997). *Principles of Colloid and Surface Chemistry* (3rd ed., 650 p). Marcel Dekker.

Lascelles, D. F. (2007). Black Smokers and the Archean Environment: An Uniformitarian Model for the Genesis of Banded Iron-Formations. *Ore Geology Reviews, 32,* 381-411. https://doi.org/10.1016/j.oregeorev.2006.11.005

Lascelles, D. F. (2017). *Banded Iron Formations to Iron Ore: an Intregrated Genesis Model*. Edition Nova Science Publishers, Inc.

Lavreau, J. (1980). *Etude géologique du Zaïre septentrional. Génèse et évolution d'un segment lithosphérique archéen*. Ph.D. Thesis, Brussels: Université Libre de Bruxelles.

Lavreau, J. (1982b). The Archaean and Lower Proterozoic of Central Africa. *Revista Brasileira de Geosciências, 12,* 187-192.

Lavreau, J. (1984). Vein and Stratabound Gold Deposits of Northern Zaïre. *Mineralium Deposita, 19,* 158-165. https://doi.org/10.1007/BF00204680

Lavreau, J., & Ledent, D. (1975). Etablissement du cadre géochronologique du Kibalien. *Annales de la Société Géologique de Belgique, 98,* 197-212.

Lavreau, J., & Navez, J. (1982). *The Geochemistry of the Archaean Greenstones of Northern Zaïre. I. Analytical Results and Statistics*. Rapp. ann. 1981-1982, Mus. roy. Afr. centr., Dépt. Géol. Min. Tervuren, 101-104.

Loughnan, F. C. (1969). *Chemical Weathering of the silicate Minerals* (154 p). American Elsevier Publishing Co. Inc.

Makuku, L. M. (2018). Caractéristiques géologiques et pétrographiques des itabirites des Monts Zatua, Nord-Est de la RDC. *Revue de Congo Sciences, 6,* 141.

Morre, E. S., & Maynard, J. E. (1929). Solution, Transportation and Precipitation of Iron and Silica. *Economic Geology, 24,* 365-402. https://doi.org/10.2113/gsecongeo.24.4.365

Okamoto, G., Okura, T., & Goto, K. (1957). Properties of Silica in Water. *Geochimica and Cosmochimica Acta, 12,* 123-132. https://doi.org/10.1016/0016-7037(57)90023-6

Parr, J., Yeats, C., & Binns, R. (2003). Petrology, Trace Element Geochemistry and Isotope Geochemistry of Sulfides and Oxides from the PACMANUS Hydrothermal Field, Eastern Manus Basin, Papua New Guinea. In C. J. Yeats (Ed.), *Seabed Hydrothermal Systems of the Western Pacific* (pp. 53-57). CSIRO Exploration and Mining Report 1112F.

Yariv, S., & Cross, H. (1979). *Geochemistry of Colloid Systems* (450 p). Springer-Verlag. https://doi.org/10.1007/978-3-642-67041-1